Final Technical Report for Grant: DE-SC0009979
"SXR-XUV Diagnostics for Edge and Core of Magnetically Confined Plasmas"

PI: Dan Stutman, Johns Hopkins University

The present report summarizes the results obtained during a one-year closing extension of DoE grant "SXR-XUV Diagnostics for Edge and Core of Magnetically Confined Plasmas", at Johns Hopkins. The extension was aimed at completing the development of a new type of magnetic fusion plasma diagnostic, the XUV Transmission Grating Imaging Radiometer (TGIR). The TGIR is an advanced version of the transmission grating imaging spectrometer design previously developed by the Johns Hopkins Plasma Spectroscopy Group [1-9].

I. Introduction

The transmission grating imaging radiometer enables spatially and spectrally resolved measurements of the XUV/VUV radiated power from impurities in fusion plasmas. Monitoring the plasma impurity radiation has been an integral part of magnetic fusion research from its beginnings. The electron temperature (T_e) in a tokamak covers a wide range, from several keV in the core, to a few eV in the edge and divertor. Furthermore, the impurities in tokamak plasmas range from low-Z (Li, B, C, O) to mid and high-Z (Fe, Cu, Mo, W), while their charge state varies from neutral to fully ionized. The tokamak impurity emission covers thus a broad spectral range and has also strong spatial gradients.

A particularly difficult region to diagnose is the divertor. The divertor acts as a power exhaust volume to the hot plasma confined in the plasma core. As the divertor heat loads increase in advanced magnetic fusion devices, it becomes essential to better understand how and where power is radiated in the divertor and how it can be manipulated to reduce the heat loads. Bolometers are traditionally used to measure the total or spectrally integrated radiated power P_{rad}, while visible or UV spectrometers are used to identify which ion species are emitting. These measurements are however often insufficient in order to distinguish which impurity emissions dominate P_{rad} in different regions of the divertor. This firstly because the bulk of the divertor impurity line emission lies in the XUV/VUV range (40-1200 Å approximately). In addition, the divertor impurity spectra are complex and can change strongly in space, because the electron temperature changes from a few eV to ~100 eV over a distance of only several cm. The picture gets even more complicated when high-Z impurities such as M or W are present. Broad spectral coverage of the XUV/VUV range *simultaneous* with cm-scale spatial resolution are thus essential in order to characterize and utilize the divertor impurity emission for plasma diagnostic.

The Transmission Grating Imaging radiometer (TGIR) is a compact and modular instrument that provides spatially resolved spectra in the XUV/VUV range, with coarse (≤10 Å) wavelength resolution, but high 1-D spatial resolution (up to ~1 cm) (Fig. 1). The basic idea

behind this design is that despite the complexity of the XUV impurity spectra, coarse spectral resolution suffices for characterization of the impurity emission when combined with high spatial resolution, absolute photometric calibration, and detailed atomic modeling.

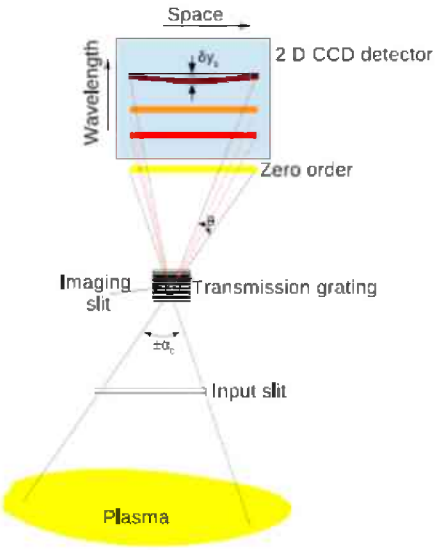

Fig. 1 Optical layout of the TGIR device.

The TGIR instrument consists of a free-standing XUV/VUV transmission grating (TG) mounted in a 1-D pinhole camera configuration, and a direct-detection XUV/VUV silicon CCD camera. The use of a direct-detection CCD in conjunction with a free-standing normal incidence TG makes for a very compact instrument and enables precise and stable photometric calibration. This in turn enables accurate measurements of the spatially and spectrally resolved radiated power P_{rad} (λ, R), for a broad range of applications: impurity species and content monitoring in the edge and divertor, validating divertor models through comparison of the predicted and measured P_{rad} (λ, R) profiles, and spectroscopic T_e and cross-field impurity transport estimates [3,6,8]. 2-D measurements of P_{rad} (λ, R, z) are also possible using two TGIRs with crossed views and tomographic reconstruction.

In addition to stand-alone impurity measurements, the spectral data from the TGIR can be used to enhance the capabilities of other diagnostics. For example, the Multi-Energy soft X-ray (ME-SXR) system on NSTX uses a set of filtered X-ray radial profile measurements in conjunction with a neural network analysis code to provide high speed (10 kHz) T_e profiles in the plasma core and edge. The sensitivity analysis of the technique has shown that its accuracy is drastically improved when including TGIR spectroscopic measurements in the neural network training, particularly in cases with large impurity influx [10].

The work within the one-year extension of the grant consisted first in the design and construction of an extended range (40-800 Å), prototype XUV/VUV radiometer having ~8 Å spectral resolution, 10° angular coverage, 0.5° angular resolution, up to 30 ms temporal resolution, and remote data acquisition capability [11]. The prototype radiometer was then

successfully demonstrated for space resolved XUV/VUV spectroscopy on the LTX tokamak at PPPL, and for a first spectroscopic study of different lithium wall conditioning methods [12].

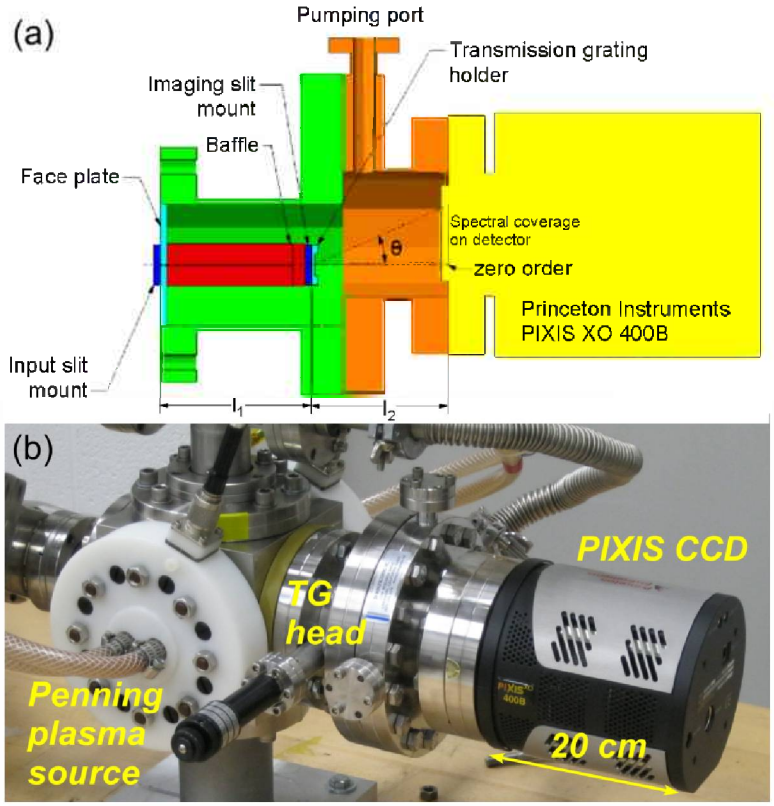

Fig. 2 a) Design of the prototype TGIR. b) TGIR mounted on the PID calibration source

II. Prototype TGIR Design

XUV spectrometers for magnetic fusion experiments have traditionally employed grazing incidence gratings as the dispersive element. However, over the past decade, free standing transmission gratings have emerged as an excellent alternative to grazing incidence gratings for building survey spectrometers in the XUV/VUV range. Not only do transmission gratings have the advantage of higher diffraction efficiency and being robust to plasma exposure, but they also lead to a simplified and compact design of the spectrometer. Fig. 2a shows the layout of the prototype TGIR diagnostic and Fig. 2b shows the instrument mounted on a laboratory PID plasma source. The instrument uses a Ta/SiC freestanding grating manufactured by NTT-ATT as the dispersive element. The grating has 5000 line-pairs/mm and active area of 1x1 mm^2. The input slit restricts the view of the plasma along one spatial direction, while the smaller imaging slit acts as a pinhole to create the 1-D image of the plasma. This image is indicated as "zero-order" in Fig 1. The 2-D CCD detector is placed so that the zero order falls outside the detector. The transmission grating is placed in proximity to the imaging slit and the grating bars oriented

parallel to the slit direction. The photons falling on the grating are diffracted perpendicular to the grating bars and form different spectrally resolved 1-D images on the detector.

The detector is a direct detection CCD camera made by Princeton Instruments, model PIXIS XO 400B. This detector has 1340×400 back illuminated pixels of size 20 μm×20 μm each, and high and nearly constant quantum efficiency in the XUV/VUV range. The simplicity and compactness of the design is evident from the fact that the whole spectrometer is contained within a volume of 6″ dia ×12″ length. The face plate in Fig. 2a isolates the spectrometer from the plasma chamber to provide a light tight environment, and also to protect the detector from debris. The rectangular input slit is mounted in front of the face plate. The incident photons from the plasma travel along the dotted line and their path is restricted by the input slit and the baffle. The light facing surfaces of the baffle have machined grooves ~50 μm deep which prevent the grazing incidence reflection of incident photons. The instrument is connected through a baffle to the experimental vacuum chamber, thus dispensing with auxiliary pumping.

With a 5000 lp/mm grating the spectrometer covers the wavelength range 40–800 Å. Grating efficiency calibrations were performed for the wavelength range 100–300 Å, which showed that the first order diffraction efficiency is essentially equal to the theoretical value of ~10%. Using the known etendue of the instrument, the absolute photometric response over the whole XUV/VUV range can thus be confidently computed from the theoretical diffraction efficiency and the CCD quantum efficiency, for calibrated measurements of $P_{rad}(\lambda,R)$.

The measured spectral resolution of the TGIR is shown in Fig. 3. With 100 μm slits the spectral resolution is around 9 Å, enabling a fairly high etendue per pixel which is beneficial for fast measurements (up to 30 ms frames). The TGIR was also tested with narrower (25 μm) slits, which provided significantly higher spectral resolution (Fig. 3), at decreased etendue. Fig. 3 shows also shows the wavelength dispersion per pixel and the maximum error in wavelength $\delta\lambda_b$, due to the use of a planar detector [11].

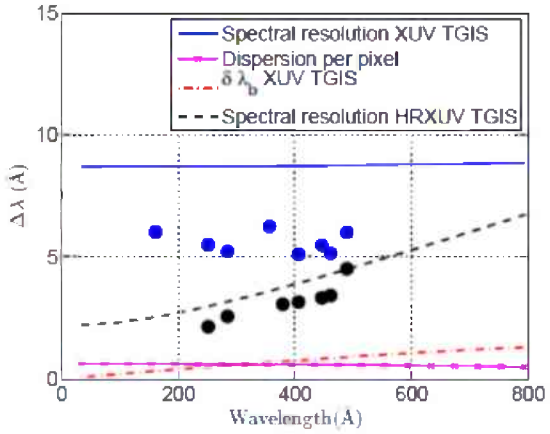

Fig. 3 Measured spectral resolution of the TGIR. The blue and black circular markers indicate the full width at half maximum (FWHM) of spectral lines measured with the low and high resolution (HR) devices respectively. The dispersion per pixel is also shown.

III. Laboratory Testing and Calibration

The TGIR was tested on a table top reflex discharge plasma source, The Penning Ionization Device (PID). Fig. 4 shows an isometric view of the PID with a quadrant removed to show the detailed structure. The TGIR testing and calibration were done operating the discharge with Ne gas at 10mTorr and Al cathodes. The input slit of the TGIR was oriented to measure the radial emission profile from the PID. Fig. 5 shows the space resolved XUV spectra measured by the TGIR using different spectral resolution and CCD binning and exposures times, under similar plasma conditions. The results indicate that high quality spectra can be obtained with exposures of only a few tens of ms, which is adequate for impurity diagnostic and transport studies in most fusion plasmas.

To test the angular resolution of the TGIR the instrument was oriented to measure the axial emission profile from the PID, when the view of the plasma was restricted by a knife edge. Fig. 6 shows the measured brightness from the Ne II 2s-2p line at 461 Å in this configuration, indicating angular resolution of ~0.5°. This translates into a spatial resolution of 0.9 cm at 1 m distance from the instrument, adequate for space resolved diagnostic in the divertor and edge.

For an approximate absolute photometric calibration of the TGIR the intensity of the Ne II $2s^2 2p^5 - 2s2p^6$ line, was compared against the measurement from an absolutely calibrated spectrometer and showed that a brightness of $1 mJ/m^2/sr$ yields 5 counts per pixel with the fast TGIR setup, again adequate for divertor and edge $P_{rad}(\lambda,R)$ diagnostic [11].

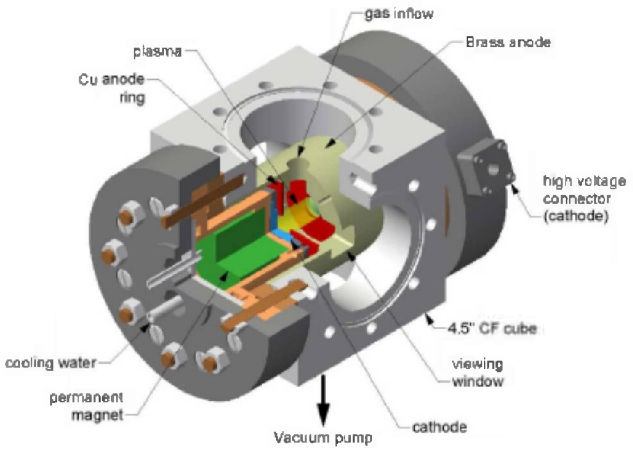

Fig. 4 PID plasma source for TGIR calibration.

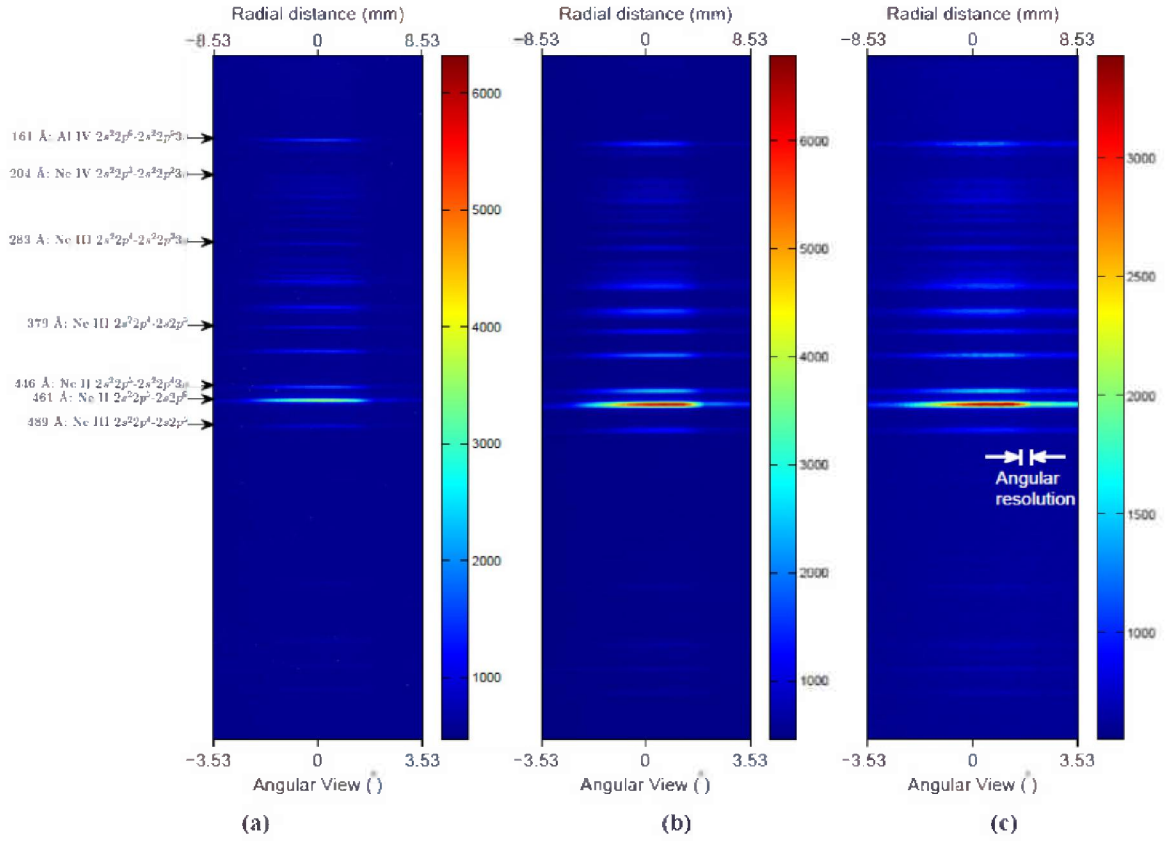

Fig. 5 TGIR XUV/VUV spectra measured along the radial direction with the PID operating with Ne gas and Al cathodes, at a current of 1.5 A. a) Space resolved spectrum measured with high resolution TGIR (25 μm slits), using exposure of ~1 s and no binning. b) Spectrum measured with the low resolution TGIR (100 μm slits) at 1.3 s exposure and no binning. c) Space resolved spectrum with the low resolution TGIR at 38.5ms exposure and 2×10 pixel binning.

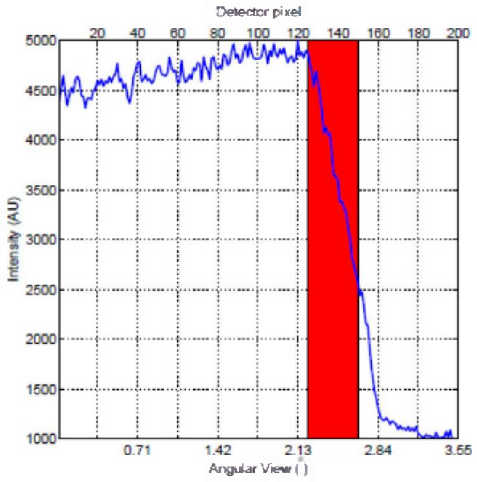

Fig. 6 Axial profile of the Ne II $2s^2 2p^5 - 2s2p^6$ line at 461 Å measured by the TGIR using a knife edge for the angular resolution assessment. The shaded box represents the theoretical angular resolution.

IV. TGIR testing and physics application on LTX

The TGIR has been tested and used for a first physics study on the Lithium Tokamak eXperiment (LTX) at PPPL [12]. LTX is a companion experiment to NSTX and serves as a flexible test bed to explore methods and techniques of using solid and liquid lithium as a first wall material. If successful, these techniques will then migrate to NSTX to improve power handling in the divertor, along with improvements in wall recycling and impurity control. The plasma regime on LTX, with T_e ~40-100eV, also provides an ideal experimental platform to test the TGIR measurement of plasma impurities in conditions similar to the NSTX divertor region.

The TGIR was installed on the LTX midplane, with a spatial view oriented tangentially across the plasma core (**Fig.** 7). Due to the machine geometry and port layout the field was restricted to several cm around the plasma axis, which limited the ability to extract spatial profiles. Since the analysis did not use the spatial information contained in the TGIR measurement, the spatial channels where binned to improve the photon statistics and signal to noise ratio (the LTX plasma emits XUV light only a few tens of ms).

A TGIR spectrum from LTX is shown in Fig. 8, with the spectral range aligned with the x-axis, and the spatial dimension arranged vertically. The image data has been smoothed to remove incident X-ray detection events, which can significantly pollute the underlying XUV/VUV spectrum. Because there are no graphite tiles in LTX, the dominant impurity species are lithium and oxygen. Furthermore, the lack of overlapping carbon emission lines allows a much more straightforward measurement of lithium emission, especially the dominant line at 135Å. The plotted spectrum shows the clear emission lines from Li III and higher charge states of oxygen, O V and O VI, though the spectral resolution is limited by the instrumental function to ~10Å, thereby blending the various groups of oxygen charge state line emission.

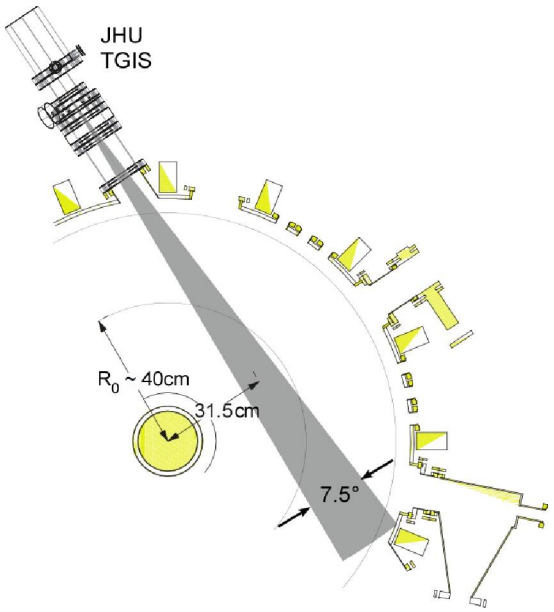

Fig. 7 Layout of the prototype TGIR on the LTX tokamak.

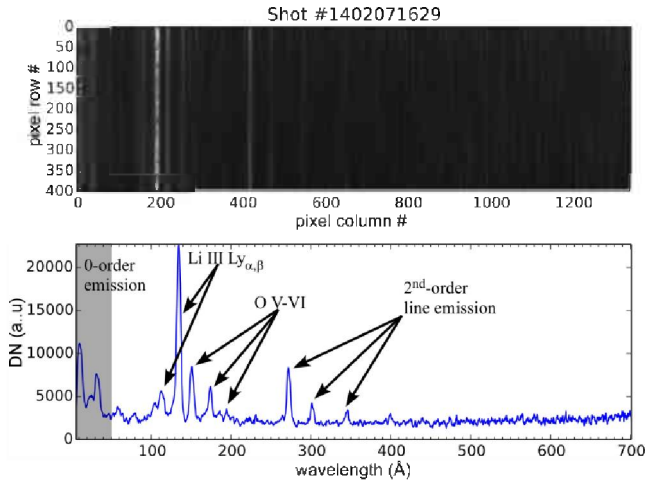

Fig. 8 TGIR spectrum from the LTX plasma.

While the instrumental width of the TGIR is too large to measure individual line emission for the blended charge states, the amplitude of fitted Gaussian curves will nonetheless provide a measure of the relative influx and concentration of lithium and oxygen impurities in the plasma. The total emission power of each Li and O spectral line is a strong function of electron temperature and particle confinement time, $n_e\tau_p$; however, the ionization energies of the dominant emitting charge states: Li III (113eV), O V (110eV), and O VI (138eV) are not too dissimilar. Therefore, using the ratios of the oxygen charge state emission lines to the primary Li III line at 135Å can largely eliminate this complex dependence on T_e and $n_e\tau_p$. Thus, comparing the values of the O/Li line ratios from each shot will isolate the effects of changes in the impurity particle source and lithium PFC pumping efficacy.

This analysis of recent experiments on LTX characterizes the effects of lithium coatings by comparing three distinct scenarios; solid semi-passivated lithium, fresh liquid lithium, and fresh solid lithium. The TGIR data show significant changes in the ratios between the lithium and oxygen impurity line emission during discharges with these varying lithium wall conditions (Fig. 9); specifically lithium coatings that have been passivated by lengthy exposure to significant levels of impurities contribute to a large O/Li ratio measured during LTX plasma discharges. The TGIR measurements of plasma discharges in LTX with hot stainless steel boundary shells and a fresh liquid lithium coating show lower O/Li impurity line ratios when compared to discharges with a solid lithium film on cool shells. The emission ratios during the liquid phase are an order of magnitude lower compared to the solid, semi-passivated lithium condition. Furthermore, the measured O/Li ratios stay steady, or even slightly decrease over the experimental run day, indicating that the pumping efficacy of the liquid lithium film is maintained. Finally, a subsequent experimental run with an unsaturated, solid lithium film shows slightly poorer pumping efficacy compared to the liquid lithium discharges, with an O/Li ratio x2-4 higher. In addition, the O/Li emission ratios slowly increase during the experimental run day, indicting a steady degradation of the solid lithium film pumping efficacy. These new

measurements help elucidate the somewhat contradictory results of the effects of solid and liquid lithium on plasma confinement observed in previous experiments which did not account for the impurity saturation level of the lithium surfaces.

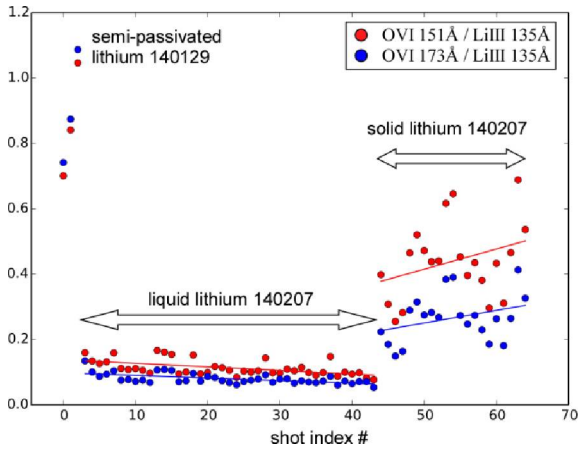

Fig. 9 O VI/Li III line ratios as a function of shot index for the solid, semi-passivated lithium, fresh liquid lithium, and refreshed solid lithium experimental campaigns.

The enhanced pumping and sequestration of liquid lithium suggests a plausible mechanism to explain the variations in pumping efficacy from previous comparisons between solid and liquid lithium observed on CDX-U, LTX and NSTX. When the lithium plasma facing component (PFC) is solid, any bonding of an impurity to the surface leaves that impurity exposed and available for future plasma surface interactions. Furthermore, as areal coverage of the reacted lithium surface grows, its pumping and impurity sequestration efficacy will decline, as shown by the increasing O/Li ratio in the above solid lithium data, as well as through extensive operational experience on LTX, CDX-U, and NSTX. Thus, solid lithium surfaces must be routinely refreshed by periodic evaporations, which effectively bury the passivated surface and maintain sequestration of the reacted impurities.

However, as demonstrated by previous LTX experimental results, a lithium substrate that is heavily saturated with impurities will readily release these impurities when melted, causing a significant impurity influx and strong degradation of the plasma performance. The increased mobility of the impurity atoms in the liquid substrate suggests that the entire lithium *volume* within some depth determined by the dissolved atomic mobility is ultimately available for plasma-surface interactions. If this volume has a high concentration of impurities, then it can act as a large net source. Conversely, if the liquid lithium film is relatively pristine, as was the case in the present TGIR/LTX study, then that specific volume, rather than just a surface layer, is available to pump and sequester the impurities via plasma-wall interactions. Instead of a slowly degrading solid lithium pumping surface, the liquid lithium film offers much higher storage capacity and more longevity for hydrogen pumping and impurity sequestration.

Therefore, to optimize the impact of liquid lithium on plasma pumping and recycling, it is essential to maintain good vacuum conditions to reduce the rate of accumulation of dissolved impurities, as well as periodically refresh any thin PFC films from a reservoir of clean lithium. Merely burying a heavily passivated film by a thin layer of evaporated lithium, which is the present prescription for NSTX-U, may be insufficient to maintain impurity sequestration for a liquid lithium first wall material.

V. Conclusion

The transmission grating instruments developed by our group for spatially resolved measurements of XUV/VUV spectra have demonstrated their utility in several scenarios, and across a broad range of plasma conditions and temperatures. The instruments can provide measurements of both charge exchange and electron excited impurity emission in the main plasma volume or in the edge. These measurements can be used independently for impurity monitoring and transport, or in conjunction with other systems for additional diagnostics, such as fast T_e profiles from the ME-SXR measurements in conjunction with neural network analysis.

The latest work in the laboratory and on LTX has demonstrated the utility of the new TGIR design for divertor-like plasma conditions. This utility has been further validated through synthetic diagnostic modeling using the OEDGE and DIVIMP divertor and impurity code. Placement of TGIR diagnostics on the NSTX-U divertor, especially coupled with an independent spectroscopic measurement of the divertor T_e and n_e, will be a valuable addition to the suite of divertor diagnostics, providing a measurement of spatially and spectrally resolved $P_{rad}(\lambda,R)$ for diagnostic of the impurity concentration and transport. The neural network analysis is estimated to be very well suited for TGIR based divertor diagnostic, while a tomographic TGIR system would enable extending this diagnostic to 2-D.

Finally, measurements of low temperature laboratory plasmas demonstrate the ability of the TGIR instrument to measure spectroscopic emission from plasmas close to the PFC surface. All of these measured quantities can then be used to validate the output of the existing 2-D and 3-D divertor codes, towards a predictive understanding of the divertor performance in present and future fusion experiments.

References

1. D. Kumar, D. Stutman, K. Tritz, M. Finkenthal, C. Tarrio, and S. Grantham, "Transmission grating based extreme ultraviolet imaging spectrometer for time and space resolved impurity measurements," Rev. Sci. Instrum. **81**, 10E507 (2010).

2. D. Kumar, D. Stutman, K. Tritz, D. Clayton, M. Finkenthal, "Modeling impurity distribution in an ST using a transmission grating based diagnostic in the EUV range," Bull. Am. Phys. Soc. **55**, *52nd Annual Meeting of the APS Division of Plasma Physics* (2010).

3. D. Kumar, D. Stutman, R. E. Bell, M. Finkenthal, D. J. Clayton, K. Tritz, B. P. LeBlanc, A. Diallo, M. Podesta, "Impurity analysis using a space resolved transmission grating based imaging spectrometer on NSTX," *Proceedings of the 38th EPS Conference on Plasma Physics, Strasbourg*, P4.047 (2011).

4. D. Kumar, A. Englesbe, D. Stutman, M. Finkenthal, "Low temperature tungsten spectroscopy on a Penning Ionization Discharge," *The 17th International Conference on Atomic Processes in Plasmas ICAPiP*, Belfast, Northern Ireland, UK, 19-22 July 2011

5. D. Kumar, A. Englesbe, M. Parman, D. Stutman, M. Finkenthal, "Low temperature tungsten and other fusion relevant element spectroscopy on a Penning Ionization Discharge," Bull. Am. Phys. Soc. **56**, *53rd Annual Meeting of the APS Division of Plasma Physics* (2011).

6. D. Kumar, M. Finkenthal, D. Stutman, R. E. Bell, D. J. Clayton, A. Diallo, B. P. LeBlanc, M. Podesta and K. Tritz, "Impurity analysis of NSTX using a transmission grating-based imaging spectrometer," *Plasma Phys. Control. Fusion*, **54**, 065010 (2012).

7. D. Kumar, D. J. Clayton, M. Parman, D. Stutman, K. Tritz, and M. Finkenthal, "Dual transmission grating based imaging radiometer for tokamak edge and divertor plasmas," *Rev. Sci. Instrum.*, **83**, 10E511 (2012).

8. D. J. Clayton, M. A. Jaworski, D. Kumar, D. Stutman, M. Finkenthal and K. Tritz, "Divertor electron temperature and impurity diffusion measurements with a spectrally resolved imaging radiometer," *Rev. Sci. Instrum.*, **83**, 10D521 (2012).

9. D. Kumar, A. Englesbe, M. Parman, M. Finkenthal, D. Stutman, "Space resolved XUV/VUV spectroscopy of low temperature plasmas," Bull. Am. Phys. Soc. **57**, *54th Annual Meeting of the APS Division of Plasma Physics* (2012).

10. D. J. Clayton, K Tritz, D Stutman, R E Bell, A Diallo, B P LeBlanc, M Podesta, "Electron Temperature Profile Reconstructions from Multi-Energy SXR Measurements using Neural Networks," *Plasma Phys. Control. Fusion,* **55** 095015 (2013).

11. D. Kumar, M. Parman, D. Stutman and M. Finkenthal, "Transmission grating based imaging spectrometers in the XUV and VUV", *Journal of Instrumentation **8**, T10002, October 2013*

12. K. Tritz, R. E. Bell, P. Biersdorfer, D. Boyle, J. Clementson, M. Finkenthal, R. Kaita, T. Kozub, S. Kubota, M. Lucia, R. Majeski, E. Merino, J. Schmitt, D. Stutman, "VUV/XUV measurements of impurity emission in plasmas with liquid lithium surfaces on LTX," *submitted Plasma Phys. Control. Fusion*, (2014).